unit circle as the temperature is reduced below the critical temperature. These analytic continuations probably correspond to metastable states.

We conclude that every physical point in the μ-T plane is regular, except the critical point, and that standard Padé-approximation procedures to the μ series should be pleasantly convergent. However, the rate of convergence near the critical point is so deceptive that it is prudent to adopt a bounding summation procedure.

ACKNOWLEDGMENT

The author is happy to acknowledge several stimulating conversations with Dr. O. Penrose during the early phases of this work.

PHYSICAL REVIEW VOLUME 161, NUMBER 2 10 SEPTEMBER 1967

Electronic Theory of Phase Transitions in Ca, Sr, and Ba under Pressure*

A. O. E. ANIMALU

Division of Applied Physics, Stanford University, Stanford, California

(Received 2 March 1967; revised manuscript received 25 May 1967)

The transitions induced by temperature and pressure between the face-centered cubic (fcc) and the body-centered cubic (bcc) phases in the alkaline earth metals—Ca, Sr, and Ba—are analyzed by computing the differences in Gibbs free energy between the two phases in the framework of the nearly-free-electron and harmonic approximations. At the absolute zero of temperature and pressure, the observed fcc in Sr and bcc in Ba were found to have the lower internal energy; in Ca, however, identical analysis led to lower energy in bcc rather than the observed fcc. An fcc-bcc transition characterized by a change in the sign of the difference in free energies in Sr at 0°K was found at a critical pressure $P_c \sim 10$ kbar; at zero pressure, it was found at a critical temperature, $T_c \sim 150$°K. Both these results agree only qualitatively with the observed $P_c \sim 36$ kbar and $T_c \sim 830$°K. Ca and Ba, already bcc at absolute zero, showed no phase transition.

I. INTRODUCTION

RECENTLY, the changes in the electrical properties and the crystal structures of the alkaline-earth metals—Ca, Sr, and Ba—under pressure have attracted considerable attention. Efforts have, however, been focused primarily on the change of the resistance with pressure and its implications for the electronic band structure of the alkaline-earth metals.[1–5] From these studies, particularly the most recent extensive band-structure calculations in the face-centered cubic (fcc) and body-centered cubic (bcc) phases by Vasvari *et al.*,[3] it has become clear that the band structures near the Fermi surface are basically nearly-free-electron-like, as previously obtained by Harrison,[6] but do not have the simple form of *s-p* bands suggested by Mott[1] and Drickamer.[2] A computation of the high-pressure electrical resistance R by Vasvari and Heine[4] on the basis of the band structure in the fcc phase has shown that the high resistance and the negative $\partial R/\partial T$ in Ca and Sr can be understood in terms of a high-pressure semimetallic state with vanishingly small Fermi-surface area, rather than the semiconducting state obtained by Altmann and Cracknell.[5] In a slightly different vein from these developments, Jerome *et al.*[7] have recently developed a theory of the transition from semimetallic states characterized by small energy gaps or small band overlaps to a new state, which they have called excitonic insulator, and for which considerable studies have been reported in the Russian literature.

In this paper we shall make a quantitative study of the transitions in the crystal structures. In pure Ca and Sr, which crystallize in the fcc phase at 0°K, temperature-induced transitions to the bcc phase have been observed at 721° and 830°K, respectively.[8] Pressure-induced transitions were first reported by Bridgman,[9,10] and the phase boundaries measured by Jayaraman *et al.*[8] up to pressures of 45 kbar. In Ca, the transition temperature T_c rises with pressure: $\partial T/\partial P \sim +3.3$°C/bar at 1 atm; in Sr, T_c drops with pressure: $\partial T/\partial P \sim -10$°C/bar. In Ba, which crystallizes in the bcc phase at 0°K, temperature-induced transitions have not been observed, but a pressure-induced transition

* This work was supported by the Advanced Research Project Agency through the Center for Materials Research at Stanford University.

[1] N. F. Mott, Phil. Mag. **13**, 989 (1966).
[2] H. G. Drickamer, Solid State Phys. **17**, 1 (1965).
[3] B. Vasvari, A. O. E. Animalu, and V. Heine, Phys. Rev. **154**, 535 (1967).
[4] B. Vasvari and V. Heine (to be published).
[5] S. L. Altmann and A. P. Cracknell, Proc. Phys. Soc. (London) **84**, 761 (1964).
[6] W. A. Harrison, Phys. Rev. **131**, 2433 (1963).
[7] D. Jerome, T. M. Rice, and W. Kohn (to be published).
[8] A. Jayaraman, W. Klement, Jr., and G. C. Kennedy, Phys. Rev. **132**, 1620 (1963).
[9] P. W. Bridgman, Proc. Am. Acad. Arts Sci. **72**, 187 (1938); **74**, 425 (1942); **81**, 169 (1952).
[10] P. W. Bridgman, Phys. Rev. **60**, 351 (1941).

to the hcp (hexagonal close-packed) phase has been reported.[11] However, in this paper we shall be primarily concerned with the fcc–bcc transitions, for which the P-V diagrams[12] and phase boundaries[8] are relatively well established experimentally. The relevant experiments will be summarized later in Fig. 7.

The thermodynamic function which determines the relative stability of two phases α and β at finite temperatures T and pressures P is the Gibbs free energy:

$$G(P, T) = H - TS, \tag{1.1}$$

where $H = U + P\Omega$ is the enthalpy, U being the internal energy and Ω the volume; and S is the entropy. It is sometimes convenient also to consider the Helmholtz free energy F, which is a function of volume and temperature, and coincides with the Gibbs function at $P = 0$:

$$F(\Omega, T) = U - TS. \tag{1.2}$$

At the equilibrium between two phases, the phase boundary is determined as a function of P and T by

$$\Delta G \equiv G_\alpha - G_\beta = 0, \tag{1.3}$$

where G_α and G_β are the values of G in the α and the β phase, respectively. For slight departure from thermodynamic equilibrium, $\Delta G > 0$ implies that the β phase has the lower free energy and is therefore more stable than the α phase. If the system was originally in the α phase, then the temperature T_c at which (1.3) is satisfied is the transition temperature for an α-β phase transition. Our task will primarily be to compute (1.2) as a function of volume and temperature in a metal from statistical mechanics, in an independent-particle model.

Recently, Harrison[13,14] and Pick and Sharma[15] have employed the pseudopotential method in the nearly-free-electron approximation for computing the internal energy due to the electronic band structure and the electrostatic interaction between the ions at 0°K. They have, however, neglected the phonon contribution to the free energy, which even at absolute zero makes a contribution to the *difference* in internal energy that is of the same order (typically 10^{-4} Rys per ion) as the electrostatic contributions, and tends to stabilize the "softer" bcc lattice. This extra contribution at 0°K will be included in the present analysis.

At finite temperatures, there has been practically no first-principles computation of the entropy difference between phases of crystal structures. However, Zener[16] has given some qualitative and, in essence, entropy-based arguments to explain the tendency to bcc at high temperatures in the transformation between α brass (fcc) and β brass (bcc). Such qualitative arguments assume, of course, that the enthalpy at 0°K is lower in the low-temperature phase. In a first-principles calculation, we have to show that a single model will give the lower enthalpy in the low-temperature phase and the lower free energy in the high-temperature phase. In this respect, our two recent papers[17,18] have gone a long way in reducing the difficult parts of the problem to the barest essentials, for we can absorb all the dependence of the internal energy of structures and the energy of the vibrating ions on the pseudopotential in a single functional, namely, the Cochran G function,[18,19] which may be determined experimentally from the phonon spectrum[19,20] of the metal. Since, however, the phonon spectra of the alkaline-earth metals have not been measured, we shall be content to evaluate the G function from the Heine–Abarenkov model potential[21,22] as described in Refs. 17 and 18, with slight modifications, if necessary, in order to obtain physically meaningful and convergent results. Then it becomes a straightforward matter to compute the phonon spectra in the fcc and bcc phases using the programs set up in Ref. 17 and to evaluate the thermodynamic functions, entropy, specific heat at constant volume, and free energy by the Houston method[23] as applied originally to cubic structures by Horton and Schiff.[24]

The conduction electrons, of course, do contribute to the entropy at finite temperatures. But, as is well known, the electronic contribution to the high-temperature specific heat is very small compared with the phonon contribution. In any case, it is practically independent of the rearrangement of the ions at constant volume, and so does not contribute to the difference in free energy. We shall therefore drop it completely from our subsequent discussion.

We begin in Sec. II by finding expressions for the separate contributions to the free energy. The calculation of the phonon spectra will be discussed in Sec. III. In Sec. IV, numerical results will be compared with experiment. In a survey of this type based on the nearly-free-electron and harmonic approximations, the errors are presumably of the same order as the energy differences, 10^{-2} to 10^{-4} Ry per ion, which we are

[11] J. D. Barnett, R. B. Bennion, and H. T. Hall, Science **141**, 534 (1963).
[12] F. P. Bundy and H. M. Strong, Solid State Phys. **13**, 81 (1963).
[13] W. A. Harrison, Phys. Rev. **129**, 2503 (1963).
[14] W. A. Harrison, Phys. Rev. **136**, A1107 (1964).
[15] R. Pick and G. Sarma, Phys. Rev. **135**, A1363 (1964).
[16] C. Zener, Phys. Rev. **71**, 846 (1947).
[17] A. O. E. Animalu, F. Bonsignori, and V. Bortolani, Nuovo Cimento **44B**, 159 (1966).
[18] A. O. E. Animalu, Proc. Roy. Soc. (London) **A294**, 376 (1966).
[19] W. Cochran, Proc. Roy. Soc. (London) **A276**, 308 (1963).
[20] R. A. Cowley, A. D. B. Woods, and G. Dolling, Phys. Rev. **150**, 487 (1966).
[21] V. Heine and I. Abarenkov, Phil. Mag. **9**, 451 (1964).
[22] A. O. E. Animalu, Tech Rep No. 3, Solid State Theory Group, Cavendish Laboratory, Cambridge, England 1965 (unpublished).
[23] W. V. Houston, Rev. Mod. Phys. **20**, 161 (1948).
[24] G. K. Horton and H. Schiff, Proc. Roy. Soc. (London) **A250**, 248 (1959).

computing, and it would be too optimistic to expect quantitative agreement with experiment. It is, however, interesting in itself to investigate what ingredients would be required in practice to understand the relation between the electronic structure and the pressure-induced transitions in the crystal structures of simple metals.

II. THE FREE ENERGY

There are two types of contributions to the separate terms U and S in the Gibbs free energy for a metal. These are the contributions due to the Fermi–Dirac assembly of conduction electrons and the contributions due to the Bose–Einstein gas of phonons arising from the quantized modes of vibration of the ion cores. Even at 0°K, the ions execute "zero-point" vibrations, so that the electronic states are, in general, coupled to the ionic motion. The adiabatic principle enables us to decouple the two systems to second order in the ionic displacement and to compute the total energy of the conduction electrons in a fixed configuration of the ions. This is the harmonic approximation, which is valid in the limit $\Theta_D/T_F \ll 1$, Θ_D being the Debye temperature and T_F the Fermi degeneracy temperature. ($\Theta_D/T_F \approx$ 0.0042, 0.0037, and 0.0027 in Ca, Sr, and Ba, respectively, at zero pressure.) In this limit, the phonon frequencies depend only on the volume and not on the temperature, and the phonons may be considered as statistically independent.

The phonon contribution to the Helmholtz free energy is given by the well-known expression[25]

$$F_{\rm ph}=U_{\rm ph}-TS_{\rm ph}, \tag{2.1}$$

where the internal $U_{\rm ph}$ reduces to the "zero-point" energy at 0°K:

$$U_{\rm ph}=\tfrac{1}{2}\sum_{\mathbf{q}s}\hbar\omega_{\mathbf{q}s}, \tag{2.2}$$

and the entropy is given by

$$S_{\rm ph}=-k\sum_{\mathbf{q}s}\ln\left[1-\exp\left(\frac{-\hbar\omega_{\mathbf{q}s}}{kT}\right)\right] +\sum_{\mathbf{q}s}\frac{\hbar\omega_{\mathbf{q}s}}{kT}\frac{1}{\exp(\hbar\omega_{\mathbf{q}s}/kT)-1}. \tag{2.3}$$

It is customary to write a single expression:

$$F_{\rm ph}=kT\sum_{\mathbf{q}s}\ln\left[2\sinh\left(\frac{\hbar\omega_{\mathbf{q}s}}{2kT}\right)\right]. \tag{2.4}$$

Here $\omega_{\mathbf{q}s}$ is the phonon frequency, $\mathbf{q}$ being the phonon wave vector and s the polarization index. $\omega_{\mathbf{q}s}$ is determined in the harmonic approximation by solving the dispersion equation

$$\sum_{\mu}[M\omega_{\mathbf{q}s}^2\delta_{\lambda\mu}-D_{\lambda\mu}(\mathbf{q})]e_{\mathbf{q}s}{}^{\mu}=0, \tag{2.5a}$$

where M is the ionic mass, and $e_{\mathbf{q}s}{}^{\mu}$ is the component along the μ axis ($\mu=1, 2, 3$) of the unit polarization vector $\mathbf{e}_{\mathbf{q}s}$. The quantity $D_{\lambda\mu}(\mathbf{q})$ is the Fourier component of the dynamical matrix, which is a sum of three contributions[26]:

(i) A Coulomb part D^C arising from the direct Coulomb interaction between the ions.

(ii) A (repulsive) Coulomb part D^R arising from the exchange overlap between the ions.

(iii) An electronic part D^E due to the polarization of the conduction-electron gas by the vibrating ions. D^E depends on the pseudopotential carried rigidly by the ion, i.e., on the electron–phonon coupling matrix.[27,28] In a cubic crystal, Eq. (2.5a) factors in the principal crystallographic directions [100], [110], and [111], so that the solution (neglecting D^R) reduces to the form

$$\omega^2(\mathbf{q}s)=\omega_c{}^2-\omega_E{}^2, \tag{2.5b}$$

where $\omega_c{}^2=M^{-1}D^C$ and $\omega_E{}^2=M^{-1}D^E$. The dependence of the solution on the pseudopotential is now given in terms of Cochran's G function by the expression[19]:

$$(\omega_E{}^2(\mathbf{q}))_{\lambda\mu}=\omega_p{}^2\sum_{\mathbf{H}}\frac{(\mathbf{q}+\mathbf{H})_\lambda(\mathbf{q}+\mathbf{H})_\mu}{|\mathbf{q}+\mathbf{H}|^2}G(\mathbf{q}+\mathbf{H}) -\omega_p{}^2\sum_{\mathbf{H}}\frac{H_\lambda H_\mu}{|\mathbf{H}|^2}G(\mathbf{H}), \tag{2.6}$$

where $\mathbf{H}$ is a reciprocal lattice vector and the G function will be defined below. The ion plasma frequency is given by

$$\omega_p=[4\pi(Ze)^2/M\Omega]^{1/2} \tag{2.7}$$

($\omega_p=6.4$, 3.9, 2.8×10^{13} sec^{-1} in Ca, Sr, Ba at zero pressure). Upon using the phonon spectra computed in the three crystallographic directions, the evaluation of (2.2), (2.3), and (2.4) is immediate by Houston's method[23,24] as described in Sec. 5 of Ref. 17 for the phonon specific heat at constant volume. This will be elaborated on later in Sec. IV.

In the one-particle (Hartree–Fock) approximation, the internal energy U_e of the conduction electrons in a fixed configuration of the ions, together with the electrostatic interaction between the ions at 0°K, can be separated, in a nonunique way by following the procedure due to Harrison[13,14] and Pick and Sharma,[15] into three parts:

$$U_e=E_{\rm es}+E_{\rm bs}+E_{\rm fe}. \tag{2.8}$$

[25] N. F. Mott and H. Jones, *The Theory of the Electrical Properties of Metals and Alloys* (Dover Publications, Inc., New York, 1936), p. 2.

[26] T. Toya, J. Res. Inst. Catalysis **6**, 161 (1958); **6**, 183 (1958).

[27] L. J. Sham and J. M. Ziman, Solid State Phys. **15**, 221 (1963).

[28] L. J. Sham, Proc. Roy. Soc. (London) **A283**, 33 (1965).

(i) E_{es} is the electrostatic energy of point ions of effective valence

$$Z^*=Z(1+\langle \mathbf{k} \mid \hat{p} \mid \mathbf{k}\rangle_{av}) \tag{2.9}$$

immersed in a uniform compensating background of the conduction electrons, where $\hat{p}$ is the projection operator introduced by Pick and Sharma which orthogonalizes the valence states to the core.

$$E_{es}=-Z^{*2}e^2\gamma/R_a \tag{2.10}$$

per ion, where $R_a=(3\Omega/4\pi)^{1/3}$ is the radius of the atomic sphere [$R_a=4.123$, 4.494, 4.661 atomic units (a.u.) in Ca, Sr, Ba at zero pressure]. The parameter γ is the Fuchs[29] constant with values 1.79172 (fcc), 1.79186 (bcc), and 1.8 (point ion in an atomic sphere).

(ii) E_{bs} is the electronic band-structure energy, which depends on the pseudopotential and the detailed configuration of the ions. We give it, as in Eq. (2.6), in terms of Cochran's G functions which we have related in Ref. 18 to Harrison's energy–wave-number characteristics. It has the form

$$E_{bs}=-\frac{4\pi Z^{*2}e^2}{2Z\Omega}\sum_{q}{}'\frac{S^*(\mathbf{q})\,S(\mathbf{q})}{\mathbf{q}^2}G(\mathbf{q}) \tag{2.11}$$

per ion. Here

$$S(\mathbf{q})=N^{-1}\sum_j \exp(-i\mathbf{q}\cdot\mathbf{R}_j)=\delta_{\mathbf{q},\mathbf{H}} \tag{2.12}$$

is the structure factor which takes completely into account the dependence of the terms on the positions of the ions at sites $\mathbf{R}_j$: It vanishes unless $\mathbf{q}=\mathbf{H}$, where $\mathbf{H}$ is a reciprocal-lattice vector. The G function for the Heine–Abarenkov model potential is

$$G(q)=\left[\frac{4\pi Ze^2(1+\alpha_{eff})}{\Omega q^2}\right]^{-2}V^b(q)\,U(q)\,\frac{\epsilon(q)-1}{1-f(q)}, \tag{2.13}$$

where $V^b(q)$ is the unscreened Fourier component of the model potential evaluated at the Fermi wave number, and $U(q)$ [$\approx V^b(q)/\epsilon(q)$] is the screened potential, $\epsilon(q)$ being the Hartree dielectric function with modifications for exchange through the factor $1-f(q)$ and for the orthogonalization charge through the factor $1+\alpha_{eff}$, as discussed in Ref. 18. In view of Shaw's[30] recent reformulation of the model potential, (2.13) can only be considered as approximately correct. Note that $G(0)=1$, so that the G function may be said to be properly normalized.

(iii) E_{fe} is the free-electron energy, which depends only on the volume, and so does not contribute to differences in the internal energy between different arrangements of the ions at constant volume. This term will not concern us further; it is needed, for example, if we wish to evaluate the absolute value of the internal energy. The term "free-electron energy" is perhaps not appropriate, since E_{fe} may depend on how the core energies are treated in setting up the pseudopotential, in which case it may depend on the arrangement of the ions. A critique of the above separation procedure has received exhaustive treatments recently.[31,32] In the model potential, of course, the core energies of the appropriate ions are taken from the atomic spectrum, which eliminates the uncertainties in *a priori* Hartree–Fock calculations, and in this case E_{fe} is independent of core rearrangement in the separation procedure.

If we collect terms, we obtain finally for the internal energy at 0°K due to the electrons in a fixed configuration of the ions, and to the electrostatic interaction between the ions, the expression

$$U_e=-Z^{*2}\left[e^2\gamma/Ra+\frac{4\pi e^2}{2Z\Omega}\sum_{q}{}'\frac{S^*(\mathbf{q})\,S(\mathbf{q})}{\mathbf{q}^2}G(\mathbf{q})\right]+E_{fe}, \tag{2.14}$$

where we have pulled out the dependence of the electrostatic and band-structure terms on Z^*. It is important to observe that the part which depends on the arrangement of ions contains Z^* as a factor. Since the G function can be determined from experiment, there are no serious objections to the use of Z^* in computing *energy differences*. As discussed earlier in connection with Eq. (1.3), we are only concerned with the zero and sign of the difference in Gibbs function. Consequently, the precise value of Z^* is unimportant, and we have used Z directly. A similar argument applies to the renormalization of the plasma frequency in (2.7) as discussed in Ref. 17, i.e., we use $(Ze)^2$ here instead of $(Ze^*)^2$.

The final expression for the Gibbs free energy in the nearly-free-electron and harmonic approximations is

$$G(p,T)=U_e+F_{ph}+p\Omega, \tag{2.15}$$

where U_e and F_{ph} are given by (2.1) and (2.14).

III. THE PHONON SPECTRA

In this section we shall discuss the computation of the phonon spectra in Ca, Sr, and Ba as a function of Ω/Ω_0, where Ω_0 is the atomic volume at zero pressure. Since this is sensitive to the choice of the pseudopotential form factors $v(q)$ required for evaluating the G function appearing in (2.6), a realistic choice of $v(q)$ has to be made in order to obtain numerical results with any physical content. We have therefore performed the calculations in two models.

The first (model A) is the straight Heine–Abarenkov model potential with the parameters in Ca, Sr, and Ba taken from Table 1 or Vasvari *et al.*,[3] and their variation

[29] K. Fuchs, Proc. Roy. Soc. (London) **A151**, 585 (1935).
[30] R. W. Shaw, Jr. thesis, Stanford University, 1967 (unpublished).
[31] S. H. Vosko, Phys. Rev. **153**, 683 (1967).
[32] L. Kleinmann, Phys. Rev. **146**, 472 (1966).

with volume incorporated simply by changing the atomic volume Ω and the orthogonality correction $\alpha_{\text{eff}}=\frac{1}{2}(R_c/R_a)$, where R_a has been defined in (2.10) and R_c is the ion core radius. The physical content of the results is found to be unchanged by including the damping factor of $\exp[-0.03\times(q/2k_F)^4]$ multiplying $V(q)$ suggested by Animalu and Heine,[33] and so we have dropped the factor altogether.

The second (model B), to which the successful results outlined in the abstract pertain, is the modification of model A described in Ref. 17. It consists of replacing A_2 with Z/R_M in order to make the $l\geq 2$ angular momentum components of the model potential *continuous* at R_M. This was found[17] to be more effective in reducing any ripples in the convergence of sums like (2.6) and (2.11), and to be as satisfactory in reproducing the electronic band structure and Fermi surfaces as model A. The differences between $v(q)$ in the two models is illustrated for Sr with $A_2=0.88$ (model A) and with A_2 replaced by $Z/R_M=0.56$ (model B) in Fig. 1. The two agree closely at small q, but at large q the smoother form of model B definitely leads to more satisfactory results in the phonon spectrum and in the internal energy differences at 0°K (to be discussed in Sec. IV). We have, however, retained both models, partly because of their respective successes in other connections,[17,33] and partly because the bulk of the computation was initially performed on model A.

For definiteness we have tabulated the Coulomb frequencies $\omega_c^2(\mathbf{q}s)$ appearing in (2.5) in Table I[34,35] for the fcc and bcc structures in units $\omega_p=1$, since in this unit, it is the same for all fcc and for all bcc structures, and the variation with volume can be incorporated easily by scaling ω_p^2 with a factor $(\Omega/\Omega_0)^{-1}$, using the values of ω_p at $\Omega/\Omega_0=1.0$ given in (2.7). We have neglected the exchange overlap contribution to (2.5), as in Ref. 17, since the core (cf. R_c/R_a) is as small in

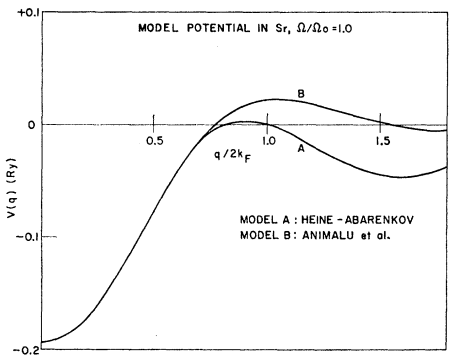

FIG. 1. The screened-model potentials in Sr at $\Omega/\Omega_0=1.0$.

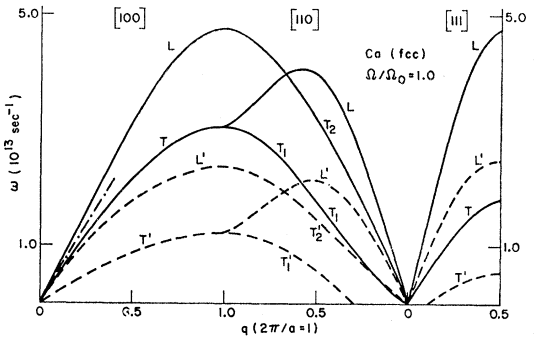

FIG. 2. Phonon dispersion in fcc Ca at $\Omega/\Omega_0=1.0$. Note: The longitudinal and transverse branches are labeled according to the polarization vectors defined in Table I. —— (backscattering), – – – (forward scattering), -·-·- (mean longitudinal sound velocity).

the alkaline-earth as in the alkali metals and Al, over the range $\Omega/\Omega_0\gtrsim 0.7$ for which (2.5) is positive.

For the electronic part we observe first that the experimental Debye temperature ($\Theta_D=230$, 171, 113°K in Ca, Sr, and Ba at $\Omega/\Omega_0=1.0$) is appreciably lower than the theoretical Einstein temperature $[\Theta_E=(\hbar/k)\omega_p/\sqrt{3}=277$, 172, 122°K in Ca, Sr, and Ba at $\Omega/\Omega_0=1.0]$ in Ca and Ba, but $\Theta_D\sim\Theta_E$ in Sr. Θ_E represents the (unscreened) restoring force when a single ion is displaced from its mean equilibrium lattice site, whereas Θ_D includes the screening action of the conduction-electron gas. We would therefore expect the electronic contribution in (2.5) to be more appreciable in Ca and Ba than in Sr. This is, in fact, the case (model B), as we shall also see in Sec. IV by comparing the absolute magnitudes of similar contributions to the internal energies at 0°K. Secondly, we find (model A) that the form factors $v(q)=\langle\mathbf{k}+\mathbf{q}\mid v\mid\mathbf{k}\rangle$ are strongly nonlocal, i.e., depend strongly on the relative orientations of the initial electronic state $\mathbf{k}$ and the final state $\mathbf{k}'=\mathbf{k}+\mathbf{q}$. We have shown in Fig. 2 the enormous differences between calculations performed with $\mathbf{k}$ parallel to $\mathbf{k}'$ (*forward* scattering for $q>2k_F$) and $\mathbf{k}$ antiparallel to $\mathbf{k}'$ (*back* scattering); the ratio of the corresponding elastic constants is nearly $\frac{3}{2}$. The Bohm-Stever[36] speed of sound is $[(\frac{2}{3}E_F)Z/M]^{1/2}\approx 3.9\times 10^5$ cm/sec, and the measured[37] mean speed of sound is $[3(1-\sigma)/(1+\sigma)\chi\rho]^{1/2}\approx 4\times 10^5$ cm/sec, σ being the Poisson ratio, χ the compressibility, and ρ the density. Each gives a mean longitudinal elastic constant lying between the two extremes of forward scattering and back scattering. However, we have used the back-scattering $v(q)$ with $|\mathbf{k}|=k_F$ throughout the calculation, since this corresponds to the minimum in the energy denominator[18] in $G(q)$. Other nonlocal effects, e.g., in the screening, were ignored. The summation in (2.6) was carried to *equal* distances of $(\sqrt{26})(2\pi/a_b)$

[33] A. O. E. Animalu and V. Heine, Phil. Mag. **12**, 1249 (1965).
[34] S. H. Vosko, R. Roger, and G. H. Keech, Can. J. Phys. **43**, 1187 (1965).
[35] L. J. Sham, thesis, University of Cambridge, 1963 (unpublished).
[36] D. Bohm and T. Stever, Phys. Rev. **84**, 836 (1951).
[37] K. A. G. Schneidner, Jr., Solid State Phys. **16**, 275 (1964).

TABLE I. ω_c^2 in units of ω_p^2. Longitudinal branches of ω_c^2 in each of the three directions [100], [110], and [111] are denoted by L, and transverse branches by T_1 and T_2 (or by T when T_1 and T_2 are identical). In the [100] direction, $\mathbf{q}=q(1, 0, 0)$, the polarization vectors are $\mathbf{e}_L=(1, 0, 0)$, $\mathbf{e}_T=(0, 1, 0)$, or $(0, 0, 1)$; in the [110] direction, $\mathbf{q}=q(1, 1, 0)$, $\mathbf{e}_L=(1, 1, 0)/\sqrt{2}$, $\mathbf{e}_{T1}=(1, -1, 0)/\sqrt{2}$, $\mathbf{e}_{T2}=(0, 0, 1)$; in the [111] direction, $\mathbf{q}=q(1, 1, 1)$, $\mathbf{e}_L=(1, 1, 1)/\sqrt{3}$, $\mathbf{e}_T=(1, -1, 0)/\sqrt{2}$, or $(1, 1, -2)/\sqrt{6}$.

	$\mathbf{q}=q(1, 0, 0)$		$\mathbf{q}=q(1, 1, 0)$			$\mathbf{q}=q(1, 1, 1)$	
$(a/2\pi)q$	L	T	L	T_1	T_2	L	T
(a) fcc							
0.1	0.9926	0.0037	0.9916	0.0009	0.0075	0.9912	0.0044
0.2	0.9710	0.0145	0.9645	0.0043	0.0312	0.9682	0.0159
0.3	0.9370	0.0315	0.9141	0.0120	0.0739	0.9399	0.0300
0.4	0.8934	0.0533	0.8354	0.0260	0.1386	0.9172	0.0414
0.5	0.8442	0.0779	0.7259	0.0472	0.2268	0.9086	0.0457
0.6	0.7940	0.1030	0.5895	0.0748	0.3357		
0.7	0.7479	0.1261	0.4395	0.1053	0.4551		
0.8	0.7107	0.1447	0.2993	0.1336	0.5671		
0.9	0.6865	0.1567	0.1981	0.1537	0.6483		
1.0	0.6781	0.1609	0.1609	0.1609	0.6781		
(b) bcc							
0.1	0.9904	0.0059	0.9892	0.0015	0.0113	0.9862	0.0080
0.2	0.9553	0.0234	0.9553	0.0056	0.0412	0.9267	0.0377
0.3	0.8971	0.0525	0.9127	0.0110	0.0784	0.7986	0.1018
0.4	0.8174	0.0923	0.8777	0.0155	0.1089	0.5897	0.2062
0.5	0.7203	0.1409	0.8642	0.0173	0.1206	0.3340	0.3340
0.6	0.6132	0.1944				0.1235	0.4393
0.7	0.5075	0.2473				0.0561	0.4730
0.8	0.4171	0.2925				0.1399	0.4311
0.9	0.3558	0.3232				0.2730	0.3646
1.0	0.3340	0.3340				0.3340	0.3340

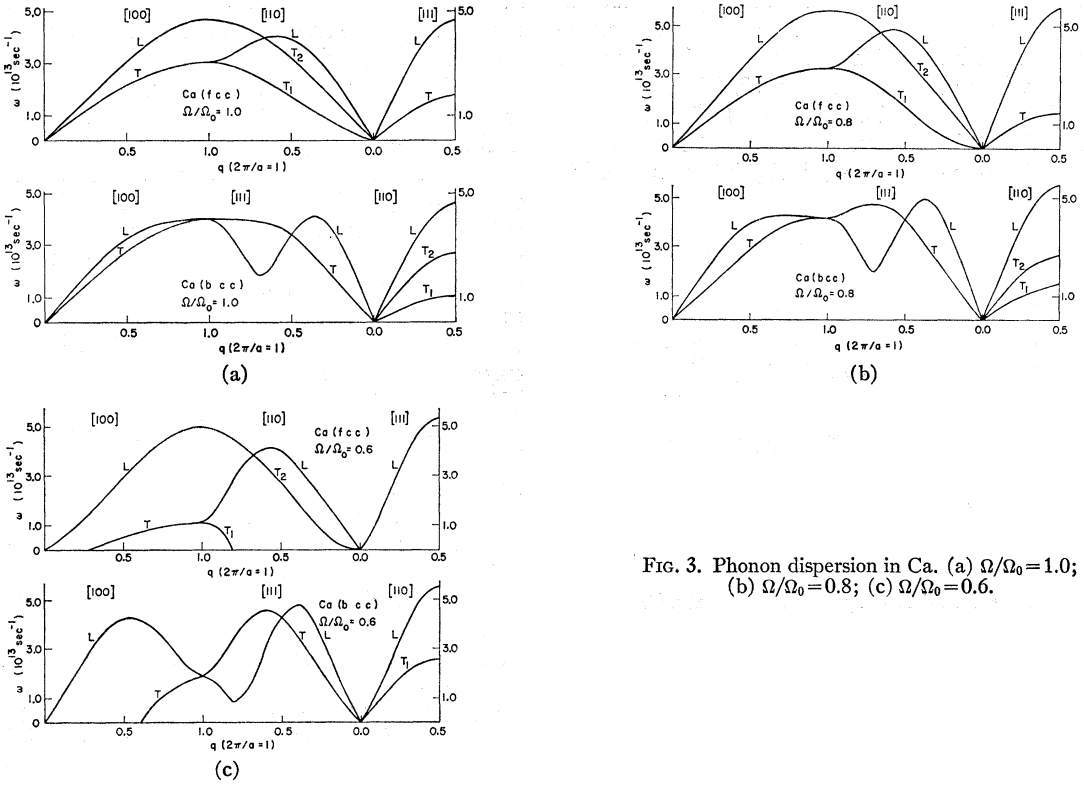

FIG. 3. Phonon dispersion in Ca. (a) $\Omega/\Omega_0=1.0$; (b) $\Omega/\Omega_0=0.8$; (c) $\Omega/\Omega_0=0.6$.

TABLE II. ω (model B) (in units of ω_p) in Sr at $\Omega/\Omega_0=1.0$. The polarization directions are exactly as in Table I. The table gives the evaluated expression (2.5).

	$\mathbf{q}=q(1,0,0)$		$\mathbf{q}=q(1,1,0)$			$\mathbf{q}=q(1,1,1)$	
$(a/2\pi)q$	L	T	L	T_1	T_2	L	T
(a) fcc							
0.1	0.0871	0.0632	0.1471	0.0326	0.0896	0.1892	0.0696
0.2	0.1774	0.1249	0.2861	0.0799	0.1787	0.3639	0.1379
0.3	0.2646	0.1837	0.4011	0.1290	0.2646	0.5020	0.1931
0.4	0.3486	0.2390	0.4822	0.1813	0.3454	0.5920	0.2294
0.5	0.4245	0.2870	0.5255	0.2349	0.4199	0.6231	0.2416
0.6	0.4902	0.3274	0.5307	0.2869	0.4861		
0.7	0.5441	0.3595	0.5049	0.3347	0.5415		
0.8	0.5841	0.3829	0.4615	0.3711	0.5829		
0.9	0.6088	0.3971	0.4196	0.3941	0.6084		
1.0	0.6171	0.4019	0.4019	0.4019	0.6171		
(b) bcc							
0.1	0.1170	0.0826	0.1937	0.0340	0.1154	0.2441	0.0911
0.2	0.2176	0.1641	0.3643	0.0682	0.2219	0.4349	0.1841
0.3	0.3101	0.2413	0.5013	0.0911	0.3042	0.5398	0.2789
0.4	0.3850	0.3116	0.5906	0.1034	0.3559	0.5426	0.3722
0.5	0.4425	0.3748	0.6218	0.1101	0.3736	0.4494	0.4494
0.6	0.4847	0.4297				0.3038	0.5021
0.7	0.5121	0.4753				0.2493	0.5307
0.8	0.5274	0.5088				0.3612	0.5397
0.9	0.5344	0.5293				0.4864	0.5383
1.0	0.5363	0.5363				0.5363	0.5363

in reciprocal lattice space, where $a_b=(2\Omega)^{1/3}$ is the bcc lattice constant. Convergence was better than 0.1% in model B, but as high as 5% or less in model A, as determined by the symmetry of the dispersion curves.

The phonon spectra (model A) are given for Ca, Sr, and Ba in Figs. 3, 4, and 5, respectively. Since all the dispersion curves turned out to be very similar to the ones in Ca, we have shown those at $\Omega/\Omega_0=1.0$, 0.8, and 0.6 in Figs. 3(a), 3(b), and 3(c), respectively, for Ca only. The computation was repeated for model B, not in its entirety, but only in Sr at $\Omega/\Omega_0=1.0$ (Table II), for the reason (see below) that here it was only in model B that we obtained the correct fcc phase with lower internal energy than the bcc at 0°K. The variation of the shapes of the dispersion curves with Ω comes entirely from the G function (Fig. 6).

The computations were terminated where the lower transverse branches become pure imaginary. In Ca and Ba this occurred for $\Omega/\Omega_0=0.7$ and for Sr at $\Omega/\Omega_0=0.7$ (fcc), 0.6 (bcc). This suggests that both fcc and bcc structures will be unstable at smaller values of Ω/Ω_0.

There are no measurements to date of either the phonon spectra or the elastic constants in Ca, Sr, and Ba. In Sec. IV, however, we shall evaluate the specific heat at constant volume, $C_v(T)$, and show that it does

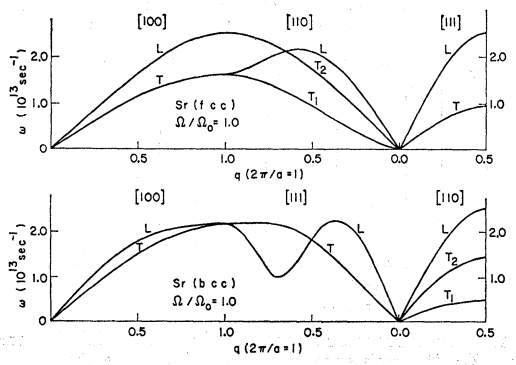

FIG. 4. Phonon dispersion in Sr at $\Omega/\Omega_0=1.0$.

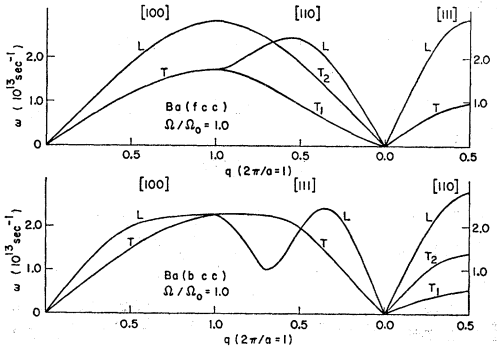

FIG. 5. Phonon dispersion in Ba at $\Omega/\Omega_0=1.0$.

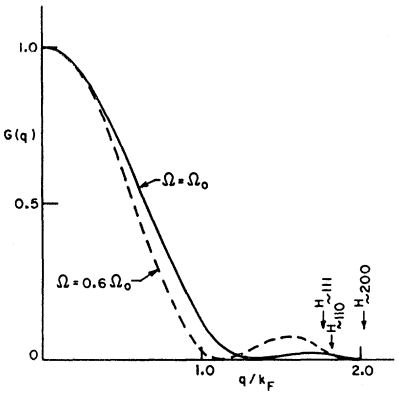

FIG. 6. Volume dependence of Cochran's G function in Ca (dimensionless units). The first three nonzero reciprocal lattice points in the fcc and bcc structures are indicated by $\mathbf{H}_{110}$ (bcc), and $\mathbf{H}_{111}$, and $\mathbf{H}_{200}$ (fcc).

have the T^3 behavior at low temperatures $T\ll\Theta_D$ and tends to the Dulong–Petit limit of $3R$ (R=the gas constant) at $T\gg\Theta_D$, as expected.

Before we proceed in the next section to the detailed computation of the free energy, it is useful to conclude this section by giving a semiquantitative version of Zener's original qualitative arguments[16] for the tendency of the fcc phase to transform to the bcc phase at high temperatures, $T\gg\Theta_D$. Let us assume that the enthalpy difference between the bcc phase and the fcc phase is positive at 0°K, i.e.,

$$\Delta H\equiv\Delta U+p\Delta\Omega>0, \tag{3.1}$$

where $\Delta X\equiv X_{\rm bcc}-X_{\rm fcc}$ for any X. Then at 0°K, Eq. (3.1) expresses the fact that the fcc phase is more stable than the bcc phase. At a finite temperature T, the equilibrium between the two phases is given by

$$\Delta G\equiv\Delta H-T\Delta S=0, \tag{3.2}$$

where ΔS comes entirely from the phonon contribution (2.3) and is practically independent of temperature. For, in the harmonic approximation,[38]

$$S\approx-k\sum_{qs}\ln(\hbar\omega_{qs}/kT)\qquad\text{for}\qquad T\gg\Theta_D, \tag{3.3}$$

so that

$$\Delta S\approx k\sum_{qs}\ln[\omega_{qs}(\text{fcc})/\omega_{qs}(\text{bcc})]. \tag{3.4}$$

The transition temperature T_c is therefore given by (3.2) as

$$T_c=\Delta H/\Delta S, \tag{3.5}$$

where for a real transition to occur we must have $T_c>0$, i.e., assuming Eq. (3.1), $\Delta S>0$. Zener made the observation that the main difference between the shear resistances of the bcc and the fcc packing of hard spheres arises in the $[1\bar{1}0]$ direction in the (110) plane: The bcc offers no resistance to a shear of this type. The elastic constant, $\frac{1}{2}(C_{11}-C_{12})$, associated with this shear is given by the slope of the lower transverse T_1 branch in the [110] direction of the phonon spectrum, which is generally higher in the fcc than in the bcc phase at zero pressure [cf. Figs. 3(a), 4, and 5]. Thus $\Delta S>0$ in (3.4) is approximately equivalent to

$$\tfrac{1}{2}(C_{11}-C_{12})_{\rm fcc}>\tfrac{1}{2}(C_{11}-C_{12})_{\rm bcc}. \tag{3.6}$$

On introducing the complementary shear constant $(C_{44})_{\rm fcc}\approx(C_{44})_{\rm bcc}$, and the anisotropy ratio

$$A=C_{44}/\tfrac{1}{2}(C_{11}-C_{12}), \tag{3.7}$$

the condition (3.6) reduces to $A_{\rm bcc}>A_{\rm fcc}$ for a transition from fcc to bcc to occur at $T\gg\Theta_D$. Zener found $A=18.7$ in β-brass (bcc) and $A=4.0$ in α-brass (fcc) to substantiate this argument. Detailed calculation to be presented in the next section shows $\Delta S>0$ at $\Omega/\Omega_0=1.0$ but not necessarily so for smaller Ω/Ω_0, for both models we have used here. From the fact that $A\equiv C_{T2}^2/C_{T1}^2$, where C_{T1} and C_{T2} are the velocities of sound for the transverse [001] and $[1\bar{1}0]$ branches in the [110] direction [given in Figs. 3(a), 4, and 5], we obtain $A_{\rm bcc}=7.7$, 9.5, 7.9 and $A_{\rm fcc}=6.3$, 6.3, 6.3 in Ca, Sr, and Ba, respectively, at $\Omega/\Omega_0=1$, consistent with $\Delta S>0$ and the occurrence of a *temperature-induced* phase transition, as expected.[8] The transitions also manifest a discontinuity in the specific heat at T_c, as will be discussed below, with $\Delta C_v(T_c)<0$, consistent with the absorption of heat at T_c.

IV. NUMERICAL RESULTS AND DISCUSSION

In this section we shall evaluate the structure-dependent parts of the free energy from the expressions

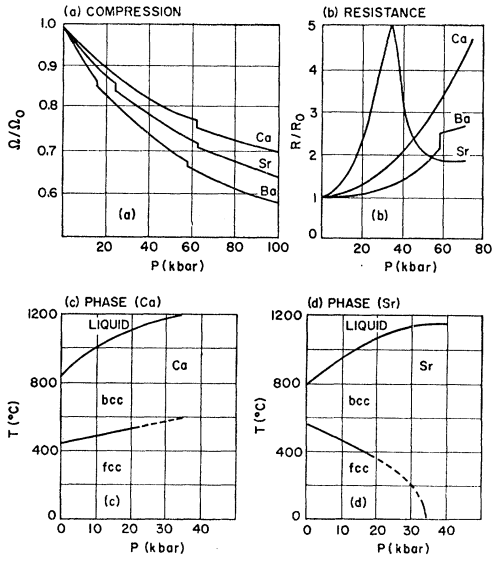

FIG. 7. Experimental results in Ca, Sr, and Ba. (a) Compression (Ref. 12); (b) resistance (Ref. 12); (c) phase diagram in Ca (Ref. 8); (d) phase diagram in Sr (Ref. 8).

[38] Reference 25, p. 20.

given in Sec. II and compare the numerical results with experiments. The relevant experiments are summarized in Figs. 7(a)–7(d): Fig. 7(a) gives the relation between the volume contraction and the pressure[12]; Fig. 7(b) gives the corresponding change in the electrical resistance, which has been discussed in Ref. 4; Figs. 7(c) and 7(d) are the fcc–bcc phase diagrams[8] in Ca and Sr, respectively. In Ref. 8, the corresponding entropy changes at the transition temperatures were quoted as $\Delta S\sim 0.08$ e.u. in Ca and $\Delta S\sim 0.23$ e.u. in Sr at 1 atm ($\Omega/\Omega_0\approx 1.0$), where the entropy unit (e.u.)$\approx\frac{1}{2}R$, R being the gas constant, so that $\Delta S\sim 0.04R$ (Ca), $\sim 0.12R$ (Sr).

At constant values of Ω/Ω_0, it is more convenient to evaluate the Helmholtz free energy $F(\Omega, T)=U-TS$, than the Gibbs free energy $G(P, T)=U-TS+p\Omega$. The part of the free energy which depends on structure may be written in the form

$$\tilde{F}(\Omega, T)=\tilde{U}-TS_{\rm ph}, \tag{4.1}$$

where the entropy part $S_{\rm ph}$ is given by (2.3), and the internal-energy part has the form

$$\tilde{U}=U_{\rm ph}+\tilde{U}_e, \tag{4.2}$$

where $U_{\rm ph}$ is the phonon "zero-point" energy given by (2.2) at 0°K, and

$$\tilde{U}_e=-Z^2\left[e^2(\gamma-1.8)/R_a+\frac{4\pi e^2}{2Z\Omega}\sum_{\rm H}{}'\frac{S^*(\mathbf{H})S(\mathbf{H})}{\mathbf{H}^2}G(\mathbf{H})\right] \tag{4.3}$$

is the reduced form of (2.14) with Z^* replaced by Z and the electrostatic energy expressed relative to the energy of an ion in an atomic sphere [$\gamma=1.8$ in (2.10)]. The evaluation of (4.3) is straightforward with the G functions known from computation of the phonon spectra described in the preceding section. The sums were performed to *equal* distances, $|\mathbf{H}|=(\sqrt{26})\times(2\pi/a_b)$ in reciprocal lattice space (Fig. 6).

TABLE III. $\tilde{U}_e$ at 0°K in Ry/ion. $\tilde{U}_e$ is the structure-dependent part of the internal energy in a fixed configuration of the ions [Eq. (4.3)]. An asterisk indicates the structure with the lower $\tilde{U}_e$.

		Model A		Model B	
	Ω/Ω_0	$\tilde{U}_e^{\rm bcc}$	$\tilde{U}_e^{\rm fcc}$	$\tilde{U}_e^{\rm bcc}$	$\tilde{U}_e^{\rm fcc}$
Ca	1.0	−0.12672*	−0.12492	−0.12082*	−0.11984
	0.8	−0.19294*	−0.18817	−0.18093*	−0.17705
	0.6	−0.28638*	−0.26707	−0.25785*	−0.24979
Sr	1.0	−0.11630*	−0.11564	−0.01904	−0.01923*
	0.8	−0.18969*	−0.18704	−0.03712*	−0.03556
	0.6	−0.30820*	−0.30087	−0.05159*	−0.04753
Ba	1.0	−0.47711*	−0.47482	−0.04976*	−0.04886
	0.8	−0.72749*	−0.72246	−0.07724*	−0.07393
	0.6	−1.19789*	−1.18658	−0.11459*	−0.11058

TABLE IV. The phonon "zero-point" energies $U_{\rm ph}$ (Ry/ion).

	Ca (Model A)	Sr (Model A)	Sr (Model B)	Ba (Model A)
Ω/Ω_0	1.0	1.0	1.0	1.0
$U_{\rm ph}^{\rm fcc}$	0.00203	0.00116	0.00108	0.00088
$U_{\rm ph}^{\rm bcc}$	0.00198	0.00112	0.00105	0.00083

To evaluate $U_{\rm ph}$ and $F_{\rm ph}$, we use the method outlined in Sec. 5 of Ref. 17. We transform the summations over $\mathbf{q}$ in expressions like (2.2) or (2.4) into an integration over the first Brillouin zone (BZ):

$$I=\sum_{\mathbf{q}s}J(\hbar\omega(\mathbf{q}s)/kT)$$

$$=\frac{N\Omega}{(2\pi)^3}\sum_{s=1}^{3r}\int_{\rm BZ}J(x_s)q^2dq\,\sin\Theta d\Theta d\phi, \tag{4.4}$$

where $J(x_s)$ is any function of $x_s\equiv\hbar\omega(\mathbf{q}s)/kT$; $q=q(\omega, \Theta, \phi)$ is the solution of the dispersion equation; $\omega=\omega_s(q, \Theta, \phi)$ for the sth branch of the $3r$ branches of the function $\omega(\mathbf{q}s)$; and q, Θ, ϕ are the spherical polar coordinates of the vector $\mathbf{q}$. The quantity N is the number of atoms, Ω is the atomic volume, and r is the number of atoms per unit cell ($r=1$ in our case). On performing the angular integration in (4.4) by Houston's method,[23,24] we obtain

$$I=\frac{N\Omega}{(2\pi)^3}\sum_s\sum_\alpha b_\alpha\int_0^{q_D{}^\alpha}q^2J(x_{s\alpha})dq, \tag{4.5}$$

where α labels the directions [100], [110], and [111], respectively, for $\alpha=1, 2, 3$; $q_D{}^\alpha$ is the maximum (Debye) wave number in the direction α. We make the approximation of replacing the BZ by a sphere of equal volume so that all the $q_D{}^\alpha$ are the same, say $q_D=(2/Z)^{1/3}k_F$, where q_D is the Debye wave number ($q_D=k_F=0.587$, 0.538, 0.519 a.u. in Ca, Sr, and Ba at $\Omega/\Omega_0=1.0$). The constants b_α are[24]: $b_1=40\pi/35$, $b_2=64\pi/35$, $b_3=36\pi/35$ for both the fcc and bcc structures. Consequently the final value of the integral (4.5) per ion is

$$I/N=(4\pi/35)[10(I_1{}^L+2I_1{}^T)$$

$$+16(I_2{}^L+I_2{}^{T_1}+I_2{}^{T_2})+9(I_3{}^L+2I_3{}^T)], \tag{4.6}$$

where

$$I_\alpha{}^{L,T}=\frac{\Omega}{(2\pi)^3}\int_0^{q_D}J(X_{\alpha L,T})q^2dq, \tag{4.7}$$

with L and T denoting the longitudinal and transverse branches of the phonon spectrum, for $\alpha=1, 2, 3$. For the various thermodynamic quantities we simply set $J(X)=kT\,\ln(2\,\sinh\frac{1}{2}X)$ for the free energy (2.4); $J(X)=kTX/2$ for the zero-point energy (2.2); and $J(x)=kx^2e^x/(e^x-1)^2$ for the specific heat $C_v(T)$ at constant volume. We shall express the entropy and

TABLE V. Specific heat, entropy difference, and free energy in Sr (model B) at $\Omega/\Omega_0=1.0$. The specific heat and the entropy differences are in units of $R=Nk$, where N is the number of ions per gram-atom; the free energy $\tilde{F}(\Omega_0, T)$ is in Ry/ion. The sign of $\Delta\tilde{F}\equiv\tilde{F}_{bcc}-\tilde{F}_{fcc}$ is also indicated. $\Delta S\equiv S_{bcc}-S_{fcc}$ was calculated from (3.3) and so is meaningful for $T>\Theta_D$.

T(°K)	$C_v^{bcc}(T)$	$C_v^{fcc}(T)$	ΔS	$\tilde{F}_{bcc}$	$\tilde{F}_{fcc}$	$\Delta\tilde{F}$
0	0	0	0	−0.01799	−0.01815	+
50	1.973	1.963	0.16	−0.01820	−0.01830	+
100	2.655	2.659	0.19	−0.01898	−0.01902	+
150	2.829	2.836	0.20	−0.02019	−0.02016	−
200	2.894	2.902	0.21	−0.02171	−0.02160	−
250	2.926	2.934	0.21	−0.02345	−0.02328	−
300	2.943	2.952	0.21	−0.02538	−0.02514	−
350	2.953	2.962	0.21	−0.02747	−0.02716	−
400	2.960	2.969	0.21	−0.02969	−0.02932	−
450	2.965	2.974	0.21	−0.03203	−0.03160	−
500	2.968	2.977	0.21	−0.03448	−0.03397	−
550	2.971	2.980	0.21	−0.03702	−0.03645	−
600	2.973	2.982	0.21	−0.03964	−0.03901	−
650	2.974	2.983	0.21	−0.04235	−0.04164	−
700	2.975	2.985	0.21	−0.04512	−0.04435	−
750	2.976	2.985(6)	0.21	−0.04796	−0.04713	−
800	2.977	2.986(4)	0.21	−0.05087	−0.04997	−
850	2.977(6)	2.987	0.21	−0.05383	−0.05287	−
900	2.978(2)	2.987(6)	0.21	−0.05685	−0.05583	−
950	2.978(6)	2.988(1)	0.21	−0.05993	−0.05884	−
1000	2.979(0)	2.989	0.21	−0.06305	−0.06189	−

$C_v(T)$ in units of $R=Nk$ (gas constant), and the free energy and "zero-point" energy in Ry/ion, where $k=6.3446\times10^{-6}$ Ry/°K. The numerical integration of (4.7) is straightforward; one interpolates the phonon spectra from tables like Table II.

In Table III the values of $\tilde{U}_e$ are given for both models A and B, at $\Omega/\Omega_0=1.0$, 0.8, and 0.6. In Table IV the "zero-point" energy U_{ph}, which is harder to compute, is shown only at $\Omega/\Omega_0=1.0$. In Table V the free energy (4.1) is given explicitly for Sr (model B) at $\Omega/\Omega_0=1.0$, together with the entropy difference ΔS_{ph} and the specific heat at constant volume, $C_v(T)$, over a wide range of temperatures: $0\leq T\leq1000$°K. In Table VI, the results for Ca, Sr, and Ba (model A) are summarized by giving only the entropy differences at 600°K, since ΔS_{ph} remains approximately the same for $T\gg\Theta_D$. The relevance of these tables to the understanding of the phase diagrams will now be discussed.

The relative stability of the fcc and bcc phases at 0°K and at $\Omega/\Omega_0=1.0$ is determined by comparing the total-internal-energy differences obtained by adding the corresponding terms in Tables III and IV. We see that both models A and B give the lower internal energy in the bcc phase for Ca and Ba, in agreement with the observed bcc phase in Ba, but not in Ca, which is fcc. In Sr, model A gives the lower internal energy to the bcc phase at $\Omega/\Omega_0=1.0$, whereas model B gives it to the fcc—the latter model being in agreement with the observed fcc phase. The contribution from the phonon "zero-point" energy turns out to be extremely small, but consistently in favor of the "softer" bcc lattice. It is also a measure of the average phonon frequency $\bar{\omega}=\sum_{qs}\omega_{qs}$, and indicates that $\bar{\omega}_{fcc}$ is generally higher than $\bar{\omega}_{bcc}$ at $\Omega/\Omega_0=1.0$. The disappointing result in Ca is not altogether unexpected, since we are using only second-order perturbation theory in the presence of a strong d potential arising from the strongly attractive

TABLE VI. Entropy differences at 600°K (model A), in units of $R=Nk$, where N is the number of ions per gram-atom and k is the Boltzmann constant.

	Ca	Ca	Sr	Sr	Ba
Ω/Ω_0	1.0	0.8	1.0	0.8	1.0
ΔS	+0.111	−0.054	+0.188	+0.033	+0.219

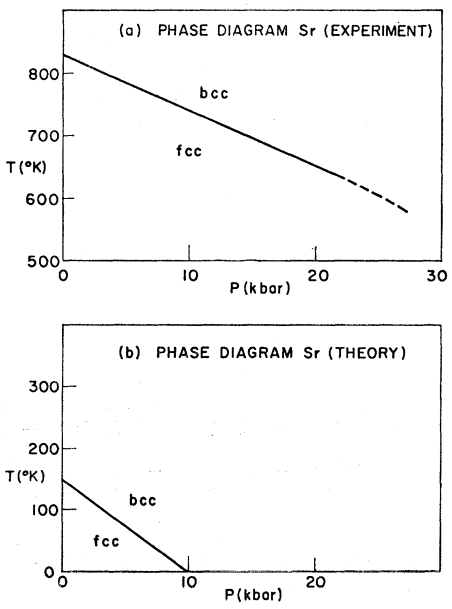

FIG. 8. Comparison between theory and experiment in Sr. (a) Experimental phase diagram; (b) theoretical phase diagram.

A_2 component in the model potential (model A). We observe, however, that Harrison (private communication) has obtained the correct fcc phase in Ca by using his point-ion model potential[39] to fit the model-A form factor $v(q)$ for $q \lesssim 2k_F$ to a smooth part $v(q) \sim \beta/q^4$ at $q > 2k_F$. The internal energy he obtained is $\tilde{U}_e = -0.1237$ Ry/ion (bcc), -0.1246 Ry/ion (fcc), which clearly indicates that the difficulty with model A definitely arises at large q. As we go to smaller Ω/Ω_0 at 0°K, model A always gives the bcc lower internal energy than the fcc—which, of course, is consistent with the tendency of the bcc to be favored at high pressures. Note, however, that the reason for this is the lower *enthalpy* associated with the bcc at high pressures; it differs from the tendency to bcc at high temperatures, which is associated with higher *entropy* in the bcc, as we have discussed in Sec. III at $\Omega/\Omega_0 = 1.0$. With model B, we obtain the interesting result that in Sr a transition from fcc to bcc occurs at about $\Omega/\Omega_0 = 0.95$ [i.e. at a critical pressure $P_c \approx 10$ kbar, from Fig. 7(a)] to be compared with the *pressure-induced* transition shown in Fig. 7(d) at $T = 0$°K and $P_c \sim 35$ kbar. Model B gives the same negative results in Ca and Ba as model A, as far as predicting the phase transition is concerned.

We turn next to the *temperature-induced* transition. The entropy differences in Table VI (model A) are consistent with the condition $\Delta S > 0$ required in (3.5) for a transition to occur at $\Omega/\Omega_0 = 1.0$. We compare, in Ca, $\Delta S = 0.11R$ (theory) with $\Delta S \sim 0.04R$ (expt), and in Sr, $\Delta S = 0.19R$ (theory) with $\Delta S \sim 0.12R$ (expt). However, model A gives the wrong signs for the enthalpy differences at 0°K, which suggests that $T_c < 0$ in (3.5), and so no transition can be predicted in this model. In model B, we again obtain interesting results for Sr. Table V indicates, from the change in the sign of the free-energy difference, that a transition occurs at $T_c \approx 150$°K from fcc to bcc for $\Omega/\Omega_0 = 1.0$, as compared with $T_c = 830$°K (expt). The phase diagram suggested by this and the pressure-induced transition considered in the preceding paragraph in Sr is shown in Fig. 8(b) (theory) for comparison with Fig. 8(a) [the experimental result of Fig. 7(d) on an expanded scale]. At 150°K, $\Delta S = 0.20R$ (theory). The agreement between theory and experiment is only qualitative: observe that $(\partial T/\partial P)_{Tc} < 0$ in both Fig. 8(a) and Fig. 8(b).

[39] W. A. Harrison, Phys. Rev. **139**, A179 (1965).

In order to evaluate the temperature-induced transition at nonzero pressure, we observe that in practice there is a slight volume change $\Delta\Omega \equiv \Omega_{\text{bcc}} - \Omega_{\text{fcc}}$ at T_c. Thus from (3.5), $T_c = (\Delta U + p\Delta\Omega)/\Delta S$, i.e.,

$$T_c(p) = T_c(0) + p(\Delta\Omega/\Delta S), \tag{4.8}$$

where $T_c(0) = \Delta U/\Delta S$ is the transition temperature at zero pressure. In Table VI, we see that ΔS in Ca is positive at $\Omega/\Omega_0 = 1.0$, but ΔS passes through a zero and becomes negative before $\Omega/\Omega_0 = 0.8$. Assume that our calculated ΔS is correct but that the model is not good enough for $T_c(0)$, this indicates that $T_c(p)$ increases with p and has gone to infinity before $\Omega/\Omega_0 = 0.8$, i.e., before 50 kbar. The measurement of the phase diagram [Fig. 7(c)] stops at about 35 kbar, so that we are not as yet in a position to test this conclusion. With the use of the Clausius–Clapeyron equation $(\partial T/\partial P = \Delta\Omega/\Delta S)$, (4.8) definitely leads to $\partial T/\partial P > 0$ in Ca with $\Delta S > 0$ if $\Delta\Omega > 0$, i.e., if there is volume *expansion* at T_c. In order to obtain results in Sr consistent with Fig. 8(b), i.e., $\partial T/\partial P < 0$, the volume must *contract* at T_c since $\Delta S > 0$.

Finally, to testify that we are indeed dealing with a phase transition—such transitions commonly being characterized by discontinuities of one sort or another—we have calculated (from Table V) the change in the specific heat $\Delta C_v(T) = -0.007R$ at 150°K (model B). A similar discontinuity is also predicted by model A at $\Omega/\Omega_0 = 1.0$ in Ca, Sr, and Ba.

In conclusion, we have shown in this paper that the transition between the fcc and bcc can be understood in the framework of the nearly-free-electron and harmonic approximations. To improve significantly on the agreement between theory and experiment in this framework we need better pseudopotentials, which, as we have argued here and elsewhere,[33] have to be determined experimentally. In an over-all sense, the present work and the band-structure calculations of Ref. 3 have been intended as a partial survey of the various steps required to understand the recent developments in high-pressure work in simple metals.

ACKNOWLEDGMENTS

I have profited greatly from conversations with Professor W. A. Harrison and Dr. V. Heine, who emphasized the need for making complete computations on the various aspects of this research.